# Barium isotopes reveal role of ocean circulation on barium cycling in the Atlantic

Stephanie L. Bates [a], Katharine R. Hendry [a,*], Helena V. Pryer [a,b],
Christopher W. Kinsley [b,c], Kimberley M. Pyle [a], E. Malcolm S. Woodward [d],
Tristan J. Horner [b,e]

[a] *School of Earth Sciences, University of Bristol, Wills Memorial Building, Queen's Road, Bristol BS8 1RJ, UK*
[b] *NIRVANA Laboratories, Woods Hole Oceanographic Institution, Woods Hole, MA 02543, USA*
[c] *Department of Earth, Atmospheric and Planetary Sciences, Massachusetts Institute of Technology, Cambridge, MA 02139, USA*
[d] *Plymouth Marine Laboratory, Prospect Place, The Hoe, Plymouth PL1 3DH, UK*
[e] *Department of Marine Chemistry and Geochemistry, Woods Hole Oceanographic Institution, Woods Hole Road, Woods Hole, MA 02543, USA*

## Abstract

We diagnose the relative influences of local-scale biogeochemical cycling and regional-scale ocean circulation on Atlantic barium cycling by analysing four new depth profiles of dissolved Ba concentrations and isotope compositions from the South and tropical North Atlantic. These new profiles exhibit systematic vertical, zonal and meridional variations that reflect the influence of both local-scale barite cycling and large-scale ocean circulation. Epipelagic decoupling of dissolved Ba and Si reported previously in the tropics is also found to be associated with significant Ba isotope heterogeneity. As such, we contend that this decoupling originates from the depth segregation of opal and barite formation but is exacerbated by weak vertical mixing. Zonal influence from isotopically-'heavy' water masses in the western North Atlantic evidence the advective inflow of Ba-depleted Upper Labrador Sea Water, which is not seen in the eastern basin or the South Atlantic. Meridional variations in Atlantic Ba isotope systematics below 2000 m appear entirely controlled by conservative mixing. Using an inverse isotopic mixing model, we calculate the Ba isotope composition of the Ba-poor northern end-member as +0.45 ‰ and the Ba-rich southern end-member +0.26 ‰, relative to NIST SRM 3104a. The near-conservative behaviour of Ba below 2000 m indicates that Ba isotopes can serve as an independent tracer of the provenance of northern- versus southern-sourced water masses in the deep Atlantic Ocean. This finding may prove useful in palaeoceanographic studies, should appropriate sedimentary archives be identified, and offers new insights into the processes that cycle Ba in seawater.
© 2017 Elsevier Ltd. All rights reserved.

*Keywords:* Barium; Barium isotopes; Ocean circulation; GEOTRACES; Atlantic

## 1. INTRODUCTION

The oceanic biological pump effectively strips nutrients and carbon out of the surface into deep waters (Riebesell et al., 2007). Silicic acid (Si(OH)$_4$) is a crucial nutrient for

organisms such as diatoms, which are responsible for exporting half of the organic matter that becomes sequestered in marine sediments (Nelson et al., 1995; Tréguer and De la Rocha, 2013). Si(OH)$_4$ and other nutrients in low-latitude regions are sourced from thermocline waters, which are fed largely from high-latitude preformed nutrients, in addition to the spatially variable fraction sourced from remineralisation (Sarmiento et al., 2004). Quantifying

past changes in the supply of nutrients, such as $Si(OH)_4$, is key to understanding past variations in the biological pump, carbon cycling and the global climate. Barium (Ba) can help us understand such processes, because there are strong, global links between Ba and other key elements in both dissolved and particulate phases: dissolved Ba shows links with $Si(OH)_4$ both vertically and spatially, and particulate Ba varies spatially with particulate organic carbon (POC) (Bishop, 1989).

The associations between dissolved Ba and $Si(OH)_4$, and particulate Ba and POC export, have led to the development of a number of Ba-based palaeoceanographic proxies. For example, Ba incorporation into carbonates (denoted by Ba/Ca) is used as a proxy for seawater dissolved Ba concentration (denoted by [Ba]) and by extension any tracer with a similarly-shaped dissolved profile such as alkalinity, $Si(OH)_4$ or DIC (Hall and Chan, 2004a,b; Lea and Boyle, 1989, 1991). Another approach builds on evidence that particulate 'excess Ba' (denoted as $Ba_{xs}$; i.e. any Ba present in particles that is unsupported by lithogenic material) correlates with POC fluxes in suspended particulates (Dehairs et al., 1991), sediment traps (Cardinal et al., 2005) and POC export (Eagle et al., 2003). These observations instigated the interpretation of $Ba_{xs}$ from marine sediment cores as a proxy for POC fluxes, allowing the reconstruction of export production and the biological pump through time (Dymond et al., 1992; Gingele and Dahmke, 1994; Nurnberg et al., 1997; Eagle et al., 2003). $Ba_{xs}$ that reaches the sediments with sequestered organic matter is assumed to be well-preserved due to the saturation of porewaters with respect to barite (Paytan and Kastner, 1996). However, quantification of nutrient cycling and export production from sedimentary Ba-based archives is still hampered by the lack of a complete mechanistic understanding of barite preservation, the linkages between $Ba_{xs}$, nutrients and POC export, and their spatially variable relationships (Hernandez-Sanchez et al., 2011).

Given the strong empirical correlations between particulate Ba and POC export fluxes, and between dissolved Si and Ba concentrations in seawater, what is known about the mechanistic controls on Ba distributions? Several explanations have been proposed for the nutrient-like behaviour of Ba in seawater, though there is now considerable laboratory (Ganeshram et al., 2003; González-Munoz et al., 2003), field (Dehairs et al., 1980; Collier and Edmond, 1984), morphological (Bertram and Cowen, 1997), geochemical (Griffith and Paytan, 2012) and thermodynamic (Monnin et al., 1999) evidence to suggest that the formation of discrete, micron-sized barite ($BaSO_4$) crystals in the water column is a biological or biologically-mediated process, and that $BaSO_4$ is the major vector of particulate Ba in the modern water column. However, these observations do not address the mechanisms behind the similar depth profiles of [Ba] and $Si(OH)_4$, which have been proposed to relate to the similar remineralisation depths of their respective carrier phases ($BaSO_4$ and opal, respectively; e.g. Broecker and Peng, 1982), or are perhaps due to the lateral advection and circulation of conservative nutrients (Horner et al., 2015) with a Ba/Si ratio set by surface processes in the high-latitudes where the water masses form

(Sarmiento et al., 2004). Although advected and organic matter-derived nutrients are traditionally labelled 'preformed' and 'regenerated' respectively, here we instead use the terms 'conservative' and 'non-conservative' to refer to these two components of Ba distributions. This choice of terminology is intended to highlight that not only organic matter remineralisation but also other processes, such as barite cycling, have potentially important effects on 'regenerated' Ba, and because there is no 'Redfieldian' (i.e. fixed) stoichiometry between dissolved Ba and organic matter that that enables back-calculation of preformed Ba from P or $O_2$ (e.g. Collier and Edmond, 1984).

Barium stable isotope analysis provides a new and powerful approach for investigating Ba cycling in seawater (Horner et al., 2015; Cao et al., 2016), as isotopic tracers are sensitive to ocean mixing *and* biogeochemistry: the precipitation of barite – a non-conservative process – preferentially incorporates the lighter isotopes of Ba (Von Allmen et al., 2010; Böttcher et al., 2012; Miyazaki et al., 2014; Nan et al., 2015), rendering residual waters depleted in Ba and isotopically 'heavier' than before precipitation occurred. In contrast, ocean mixing – a conservative process – does not fractionate isotopic distributions; resultant concentrations and isotopic patterns follow predictable isotopic mixing schemes (Hoefs, 2015). Hence, the information provided by seawater Ba isotopes, when used in combination with [Ba], can shed light on whether variations in [Ba] are driven by conservative mixing of different water masses or by non-conservative barite cycling, including both the formation and dissolution of particles via lateral and vertical transport. Only a few data exist for the isotopic composition of barium in seawater (Horner et al., 2015; Cao et al., 2016), and they show that isotopic variations reflect a combination of ocean circulation and barite cycling, with the latter evidenced by the presence of Ba-depleted, isotopically-heavy subsurface waters. A South Atlantic profile showed that, in the deep ocean, Ba isotope values are largely a function of the circulation of major water masses falling on a conservative mixing line between Antarctic Intermediate Water (AAIW), North Atlantic Deep Water (NADW) and Antarctic Bottom Water (AABW), with end-members likely determined by barite cycling in high latitude surface waters (Horner et al., 2015). A Ba isotope profile from the East China Sea illustrated that freshwater input can also influence the Ba isotopic composition of near-surface seawater, with Ba cycling in the upper water column dominated by the removal of lighter isotopes onto particles (Cao et al., 2016).

The main aim of this study is to investigate water column Ba concentrations and isotopic distributions vertically, zonally and meridionally within the Atlantic. We use these data to examine the impact of $BaSO_4$ precipitation and dissolution on Atlantic Ba cycling and to quantify the relative mixing proportions of northern- and southern-sourced water masses using new seawater depth profiles from both the eastern and western basins. Firstly, we use the isotopic composition of dissolved Ba in seawater to investigate subtle near-surface variations in Ba concentrations, and its decoupling from Si, in the tropical North Atlantic. Secondly, we use seawater Ba isotopes to trace the proportion

of deep ocean variation that is attributable to lateral advection (conservative mixing) versus barite cycling (and other non-conservative vertical processes) in these tropical locations. Lastly, we compare our new tropical North Atlantic data with profiles from the South Atlantic to investigate the extent to which basin-scale Ba distributions are driven by mixing, as opposed to barite cycling.

## 2. METHODS AND MATERIALS

### 2.1. Oceanographic setting

We present data from the South and tropical North Atlantic, which are both influenced by similar water masses at different stages of the Atlantic meridional overturning circulation (Talley, 2013). In the South Atlantic, the water column is composed of southern-sourced AABW (below ~3500 m), southward flowing NADW (~2000–3500 m), Upper Circumpolar Deep Water (core at ~1500 m), AAIW (core at ~600 m) and a mixture of Subantarctic Surface Water (SASW) and Subtropical Surface Water (STSW). In the Equatorial Atlantic, AABW occurs below ~4000 m, AAIW at ~1000 m (mixed with Mediterranean Water), NADW below ~1500–2000 m, and tropical mode and surface waters subduct to form the thermocline (Talley et al., 2011).

### 2.2. Sample collection

Seawater collection and processing procedures for samples from the South Atlantic (D357/GA10E; Oct-Nov 2010) are discussed in Horner et al. (2015). Samples from the tropical North Atlantic (JC094; Oct-Nov 2013) were collected using Niskin bottles attached to a CTD rosette system, filtered cleanly through a 0.2 micron Acropak filter (Pall Life Sciences) and samples for Ba analysis were acidified (0.1 % v/v; pH ≈ 2.0) the same day using concentrated hydrochloric acid (HCl Romil UpA). Samples were stored in a cool container (+4 °C) for transport back to the UK. Sampling stations are shown in Table 1.

Temperature, conductivity and fluorescence were measured using a Sea-Bird (SBE) 9*plus* with a Chelsea Technology Group (CTG) Aquatracka MKIII fluorimeter, and data were post-processed using SBE Data Processing (V7.20 g) software. Salinity was calculated from conductivity, and calibrated on board using bottle samples measured using a GuildLine Autosal salinometer and with Autosal software (2009). Dissolved oxygen was measured using an SBE 43 dissolved oxygen sensor mounted on the CTD and was calibrated using bottle measurements, which were carried out on board by the Winkler titration method using a Ω-Metrohm 848 Titrino plus unit with potentiometric end point detection (Carritt and Carpente, 1966; Robinson, 2014).

Additional unfiltered samples were collected for nutrient analysis and frozen at −20 °C for transport back to the UK. Nitrate + nitrite, nitrite, silicate, phosphate and ammonium were analysed using a Bran and Luebbe 5 channel segmented flow autoanalyser (Plymouth Marine Laboratories, UK) and high-resolution colourimetry (Brewer and Riley, 1965; Kirkwood, 1989; Grasshoff et al., 1999; Zhang and Chi, 2002). Samples were defrosted back on land for 48 hours at room temperature in darkness before being analysed alongside a certified nutrient reference material produced by KANSO Technos, Japan. The KANSO Technos reference materials are analysed on a daily basis as part of regular analytical protocols allowing the results stated here to have an accuracy of 2 % or better when compared to these reference concentrations. By adopting analytical methods and techniques according to GO-SHIP protocols, improvements and checks are made to ensure the analytical accuracy of nutrient analyses. Precision is again at 2 % (or better) when this is determined along side regular sample analyses. The standards used are all high-quality materials, the highest standard concentration is always greater than the highest sample concentration, and a linear slope of standards is ensured, to allow full confidence in the reported sample concentrations.

### 2.3. Barium isotope analysis

Seawater Ba concentrations and isotopic compositions were measured at the NIRVANA Lab at Woods Hole Oceanographic Institution (WHOI) using a method similar to that of Horner et al. (2015), which consists of double spiking, co-precipitation and ion-exchange chromatography followed by Ba isotope analysis via MC-ICP-MS (multiple-collector inductively-coupled plasma mass spectrometry). A new double spike composed of roughly equal proportions of $^{135}$Ba and $^{136}$Ba was used instead of the $^{135}$Ba-$^{137}$Ba double spike previously described by Horner et al. (2015); see Supplement for spike composition. The new choice of spike combination was optimised to minimize the impact of interferences from Xe – present as a trace impurity in the Ar carrier gas – found on *m/z* 136 (Xe, Ba, Ce) during MC-ICP-MS analysis.

Table 1
Locations of CTD profiles used in this study.

| Cruise | CTD number | Station | Latitude | Longitude | Water depth (m) |
|---|---|---|---|---|---|
| JC094 | CTD002 (CTD2) | 2 | 9° 17.1′N | 21° 38.0′W | 4524 |
| JC094 | CTD005 (CTD5) | 39 | 10° 51.8′N | 44° 29.5′W | 5161 |
| JC094 | CTD006 (CTD6) | 44 | 15° 16.2′N | 48° 15.6′W | 4183 |
| D357 | CTD025 (CTD25)[a] | 6 | 39° 59.4′S | 0° 55.2′E | 4927 |
| D357 | CTD013 (CTD13) | 3 | 36° 27.6′S | 13° 23.4′E | 4894 |

[a] From Horner et al. (2015).

Barium concentrations were estimated from dissolved [Si] values and an appropriate amount of $^{135}Ba$-$^{136}Ba$ double spike was added to 5 ml of seawater to achieve roughly equal proportions of spike- and sample-derived Ba in the spike-sample mixture. In accordance with GEOTRACES protocols (Cutter et al., 2010), additional ultra-pure HCl was added to the tropical North Atlantic samples at WHOI to achieve a final HCl concentration of 0.024 M (pH <2). Spike-sample mixtures were refluxed at +60 °C for 24 hours, allowed to cool to room temperature, then co-precipitated through the addition of 350 µl of 1 M $Na_2CO_3$ solution in 50 µl increments (Foster et al., 2004). After centrifugation and decantation of residual seawater, precipitates were dissolved in ~2 M HCl, dried, and resuspended in 250 µl of 2.3 M HCl for ion-exchange chromatography. Purification of Ba was achieved by passing samples twice through 500 µl of AG 50 W-X8 (200–400 mesh) cation exchange resin that was precleaned and conditioned with 6 M and 2.3 M HCl, respectively. Non-Ba matrix elements were eluted with 2.3 M HCl, followed by Ba elution using 2 M nitric acid ($HNO_3$). Purified samples were subsequently dried, to oxidize any resin-derived organic material that may have co-eluted with Ba – dried again, and finally re-dissolved in 2% $HNO_3$ for mass spectrometric analysis.

Samples were analysed for barium isotope compositions at the WHOI Plasma Facility using a Thermo Neptune MC-ICP-MS operated in low-resolution mode, fitted with 'Regular'- and 'X'-type sampler and skimmer Ni interface cones, respectively. Samples were aspirated at ~120 µl/min using an Elemental Scientific PFA µFlow nebulizer, via a CETAC Aridus II desolvator, and admixed with 3–5 ml/min $N_2$ gas to reduce $BaO^+$ formation which was ≤0.1 % during Ba ionisation (Miyazaki et al., 2014). Baseline-corrected ion beams corresponding to m/z 131 (Xe), 135 (Ba), 136 (Xe, Ba, Ce), 137 (Ba), 138 (Ba, La, Ce), 139 (La) and 140 (Ce) were measured simultaneously by 40 × 4.194 s integrations at sample-derived Ba concentrations of around 20 ng/ml; $Ba^+$ transmission efficiencies were generally ≥1 %. Barium isotope compositions were calculated in MATLAB using the three-dimensional geometric interpretation of the double spike problem (Siebert et al., 2001). In this interpretation, the x-, y-, and z-axes are defined by $^{138}Ba/^{135}Ba$, $^{137}Ba/^{135}Ba$ and $^{136}Ba/^{135}Ba$, and interference corrections for Xe, Ce, and La were performed via the nested iterative approach described in Horner et al. (2015). Sample-derived Ba concentrations were calculated based on the instrumental mass bias-corrected $^{138}Ba/^{135}Ba$ ratio (noting that most $^{135}Ba$ is spike-derived) and a priori knowledge of the spike added to each sample. Isotopic compositions are reported in the δ-notation relative to National Institute of Standards and Technology (NIST) Standard Reference Material 3104a (Ba):

$$\delta^{138/134}Ba_{NIST} = \left\{ \frac{\left(\frac{^{138}Ba}{^{134}Ba}\right)_{sample}}{\left(\frac{^{138}Ba}{^{134}Ba}\right)_{NIST SRM 3140a}} - 1 \right\} \times 1000 \qquad (1)$$

Isotopic uncertainties are reported as the larger of either the long-term 2 × SD (Standard Deviation) uncertainty on sample unknowns (±0.03 ‰, n = 8) or the pooled internal

2 × SE (Standard Error) of repeat sample measurements (median number of replicate analyses = 4), as described in Horner et al. (2015).

Blanks were monitored by passing aliquots containing ~1 ng of Ba double spike through the procedures described above and treating as sample unknowns. The mean analytical blank (from reagents and ion-exchange chemistry) was measured as 11 ± 8 pg (mean ± 1 SD; n = 4) and the procedural blank (co-precipitation plus analytical blank) was determined as 726 ± 124 pg (mean ± 1 SD; n = 6). All seawater Ba concentration data were procedural-blank corrected but Ba isotope data were not as the small proportion of blank-derived Ba in seawater samples was deemed unlikely to alter Ba isotope compositions outside of long-term uncertainty (±0.03 ‰; Horner et al., 2015). Additional details regarding the reporting of uncertainty are presented in the Supplementary information.

## 3. RESULTS

### 3.1. Temperature, salinity, oxygen and nutrient profiles

The potential temperature and salinity measurements show typical profiles for the South Atlantic and tropical Atlantic sites, with marked latitudinal differences above 3000 m water depth. Near-surface and subsurface temperatures are over 15 °C warmer in the tropics than the South Atlantic, and significantly more saline (Fig. 2A and B). The oxygen profiles from the tropical Atlantic sites show a pronounced minimum centred on approximately 500 m water depth, absent from the South Atlantic sites, and higher oxygen levels at depth than at 40°S (Fig. 2C).

Nutrients showed expected concentration profiles (Fig. 2D and F), with low concentrations at the surface as a result of biological uptake, and higher values at depth
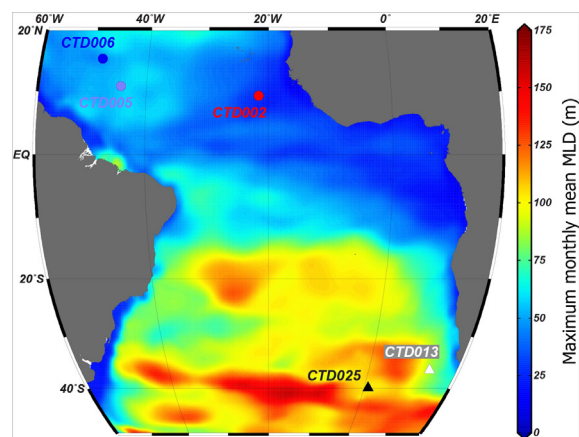


Fig. 1. Map showing locations of seawater profiles: CTD002, CTD005 and CTD006 (stations 2, 39 and 44, respectively) from cruise JC094; CTD013 and CTD025 (stations 3 and 6 from cruise D357/GA10E); CTD025 data from Horner et al., 2015. Colour contours show maximum mixed layer depths (calculated from the monthly means) from National Oceanographic and Atmospheric Administration Monthly Isopycnal & Mixed-layer Ocean Climatology (Schmidtko et al., 2013). Produced using Ocean Data View (Schlitzer, 2000).
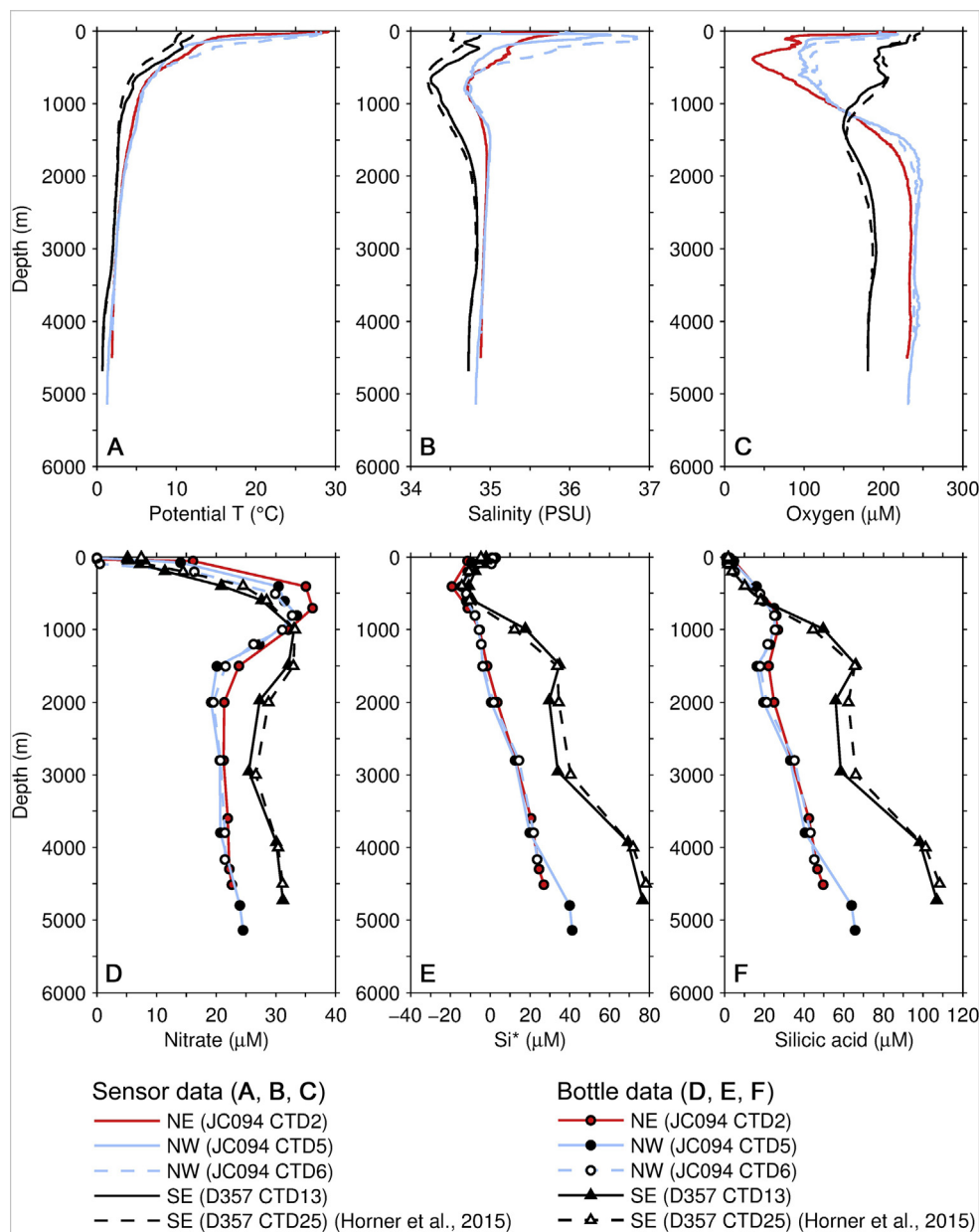
Fig. 2. Water properties at the CTD stations used in this study: (A) potential temperature; (B) salinity; (C) oxygen; (D) nitrate; (E) Si*; and (F) Si(OH)$_4$ concentration. The figure legends apply to all subsequent figures.

as a result of lateral transport of conservative nutrients and regeneration. Regenerated nutrients are represented by N* (not plotted; $N^* = NO_3^- - 16PO_4$) and Si* (Fig. 2E) where $Si^* = [Si(OH)_4] - [NO_3] + dN^*$ and the denitrification correction $d = 1$ for $N^* < -3\ \mu M$ ($d = 0$ otherwise) (Gruber and Sarmiento, 1997; Sarmiento et al., 2004). No denitrification correction was required for the tropical Atlantic samples. Si* is only conserved when remineralisation (or uptake) processes release (or take up) Si(OH)$_4$ and NO$_3$ in a 1:1 ratio, which is not the case in regions of the Southern Ocean where AAIW and mode waters are formed as a result of strong nutrient uptake by iron-limited diatoms (Si(OH)$_4$:NO$_3$ uptake ratio ∼4:1; Brzezinski et al., 2002;

Sarmiento et al., 2004). Hence, Si* is a powerful tracer of Southern Ocean intermediate depth waters, and can be used to pinpoint AAIW at ∼1000 m depth in our North Atlantic depth profiles (Fig. 2).

### 3.2. Barium and barium isotopes

Water column Ba concentrations from our new seawater profiles show the now well-established vertical fractionation of [Ba], with lower values in surface waters (∼40 nM) and higher values at depth (∼80 nM for the tropical Atlantic profiles and ∼100 nM for the new Southern Atlantic profile; Fig. 3; Supplementary information). [Ba] increases
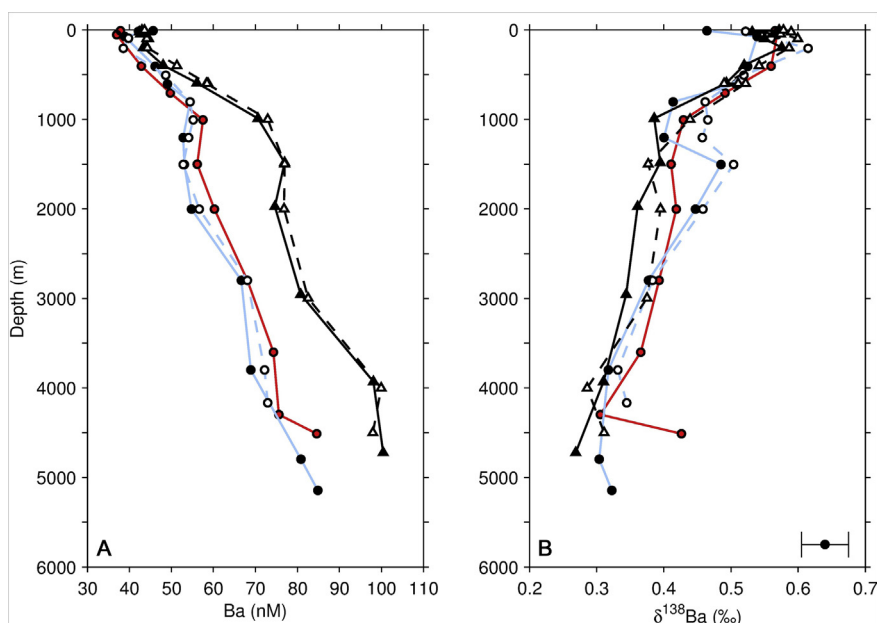
Fig. 3. (A) Barium concentrations and (B) barium isotopic compositions of the seawater samples analysed in this study. Tropical Atlantic data are plotted in red (eastern tropical) and blue (western tropical) with circle symbols, South Atlantic data are plotted in black with triangle symbols. Open triangle symbols and black dashed curves show previously-published data from the southeast Atlantic at 40°S (Horner et al., 2015). Error bar shows representative ±2SD (±0.035 ‰). The uncertainties on the barium concentrations are within the size of the symbols. See Fig. 2 for legend. (For interpretation of the references to colour in this figure legend, the reader is referred to the web version of this article.)

down the water column from ∼1500 m to 5000 m in all of the new profiles; the tropical Atlantic profiles show a slight increase of <5 nM at ∼1000 m, before declining again towards the subsurface. The shallower samples of the profiles, above ∼50 m, show that [Ba] increases slightly by ∼5 nM towards the surface. The $\delta^{138}$Ba values generally mirror [Ba], becoming progressively lighter as [Ba] increases, in good agreement with the previously-published South Atlantic $\delta^{138}$Ba profile (Horner et al., 2015). The tropical Atlantic $\delta^{138}$Ba data differ from the published South Atlantic profile in two respects. Firstly, surface $\delta^{138}$Ba profiles show heavier values at approximately 200 m (∼+0.6‰), followed by a decline of ∼0.1 ‰ towards lighter values at the surface in the tropical Atlantic samples only (Fig. 3). Secondly, there is a divergence in both [Ba] and $\delta^{138}$Ba between the tropical northwest and northeast Atlantic samples in the mid-depths, centred around a core at approximately 1500 m.

## 4. DISCUSSION

### 4.1. Ba* (barium star)

These new [Ba] and $\delta^{138}$Ba profiles, especially when assessed in the context of a previously published South Atlantic depth profile (Horner et al., 2015), provide a new insight into the relative roles of different processes that affect Atlantic Ba cycling: conservative versus non-conservative barium, the depth ranges of organic matter and barite remineralisation, and water mass mixing. These

processes can be further quantified by combining measurements of $\delta^{138}$Ba with Ba*, which is defined as the difference between *in situ* and predicted [Ba]:

$$Ba^* = [Ba]_{insitu} - 0.6296(\pm0.0022) * [Si(OH)_4]_{insitu} - 38.63(\pm0.07) \quad (2)$$

This formulation of Ba* is based on a York Regression of 1505 globally-distributed [Ba]–[Si] measurements from the GEOSECS expeditions (Geochemical Ocean Sections; e.g. Craig and Turekian, 1980), and differs slightly from the formulation used by Horner et al. (2015), which was based only on GEOTRACES-era co-located [Ba]–[Si] measurements from the South Atlantic. Regardless, the absolute values of Ba* are essentially arbitrary – the utility of Ba* is derived from the shape of the depth profiles. Vertical profiles of Ba* that vary with depth arise from subtle variations in the integrated histories of Ba and Si cycling. These variations relate to differences in the ventilation of preformed water masses, as well as the differing uptake and remineralisation processes of the two elements: barite precipitation and dissolution affects the cycling of Ba but not Si, whereas biological opal formation and dissolution impacts the cycling of Si but not Ba. For example, the water column profiles of Ba* show more negative values in the mesopelagic zone, in both the North and South Atlantic, which trend towards more positive values below approximately 2000 m before become more negative again below 3000 m (Fig. 4). The shapes of these profiles arise as a result of sampling different water masses with different physiochemical properties, locations of origin and ventilation ages.
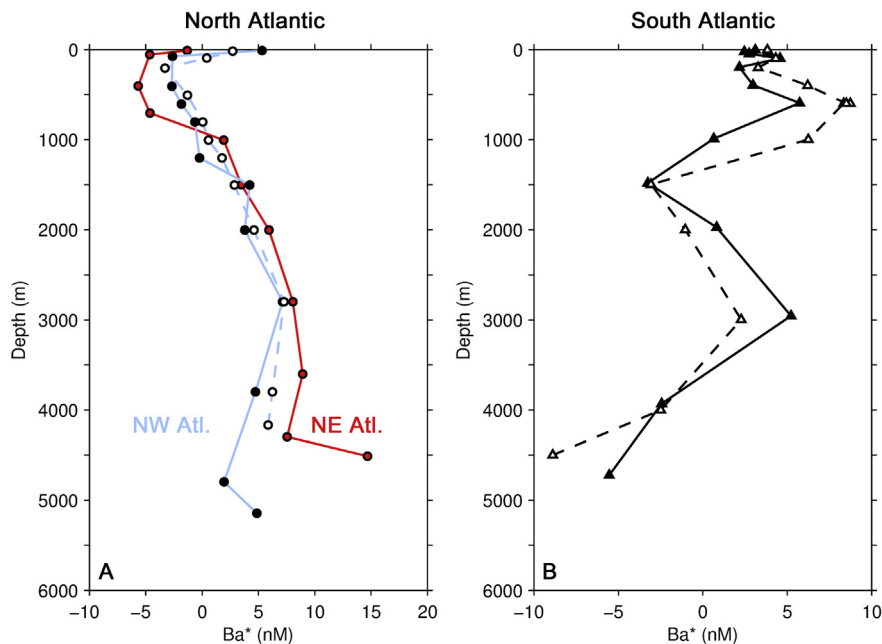
Fig. 4. Ba* plotted against depth for (A) the eastern tropical Atlantic (red) and western tropical Atlantic (blue) and (B) the South Atlantic, including previously-published data from the southeast Atlantic at 40°S (open triangle symbols and black dashed curves; Horner et al., 2015). See main text for details on how Ba* is calculated. See Fig. 2 for legend. (For interpretation of the references to colour in this figure legend, the reader is referred to the web version of this article.)

## 4.2. Surface and near-surface cycling of barium

The depth profiles of Ba* and $\delta^{138}$Ba (Figs. 3 and 4) suggest that there are marked latitudinal differences in the sub-surface processes which influence the barium cycle in the Atlantic, with a gradient in Ba* between latitudes and more heterogeneous $\delta^{138}$Ba near-surface values in the tropics compared to the South Atlantic. Of particular interest are the heavy near-surface isotopic values that trend lighter towards the surface in the North Atlantic, compared to the relatively homogeneous near-surface waters of the South Atlantic at 40°S (Fig. 4; Fig. 5; Horner et al., 2015) – this could potentially relate to differences in biological production (Tilstone et al., 2015), or to differences in the physical structure of the mesopelagic layer between the North and South Atlantic.

The heavy Ba isotope values in the sub-surface (relative to deeper waters) throughout the Atlantic are likely a result of barite formation, which preferentially incorporates isotopically-light Ba (Von Allmen et al., 2010), thus rendering residual seawater isotopically heavier and depleted in Ba. We can calculate an apparent fractionation factor ($\varepsilon'$) for barite formation in the mesopelagic and near-surface layers by solving the following equations using iterative linear regression (Marquardt–Levenberg algorithm), assuming closed or open fractionation respectively:

$$\delta^{138}\text{Ba} = \varepsilon' \ln([\text{Ba}]) + c$$
$$\delta^{138}\text{Ba} = \varepsilon'([\text{Ba}]/[\text{Ba}]_0) + c \tag{3}$$

where $[\text{Ba}]_0$ is the barium concentration of the water supplying the mesopelagic layer (after Varela et al., 2004) and c is the intercept (for more details, see the Supplementary information). Using this method, the apparent fractionation factor is calculated to be $-0.34 \pm 0.06\,‰$ (closed) or $-0.45 \pm 0.08\,‰$ (open) for the North Atlantic, and $-0.28 \pm 0.03\,‰$ (closed) or $-0.39 \pm 0.04\,‰$ (open) for the South Atlantic (uncertainties represent the standard error). Whilst these values agree well with previous estimates of Ba isotopic fractionation during barite formation in the laboratory (Von Allmen et al., 2010), these estimates are likely to underestimate the true fractionation factor as the simple assumptions of the fractionation models are often violated in complex oceanic settings. Moreover, the study of Cao et al. (2016) identified that the $\Delta^{138}$Ba offset between particles and seawater was significantly larger than estimated here using Rayleigh-type fractionation models.

Barite formation is likely associated with organic matter decomposition by heterotrophic bacteria, and high particulate Ba$_{xs}$ has been seen to be associated with organic matter remineralisation and oxygen consumption at the top of the mesopelagic layer (Cardinal et al., 2005; Jacquet et al., 2007, 2008; Dehairs et al., 2008). The oxygen minimum (which mirrors the apparent oxygen utilisation and is more pronounced in the tropics) and chlorophyll maximum occur at different depths in the two locations (Fig. 5), potentially contributing to differences in sub-surface Ba* and $\delta^{138}$Ba profiles. Biological net community production at 40°S is markedly higher than in the North Atlantic (Tilstone et al., 2015), and variations in organic matter availability, and hence barite formation, could explain the sub-surface latitudinal differences observed here. However, mass balance considerations suggest that, whilst it is important for particulate barite formation, Ba directly associated with organic matter is likely to be unimportant in terms of set-
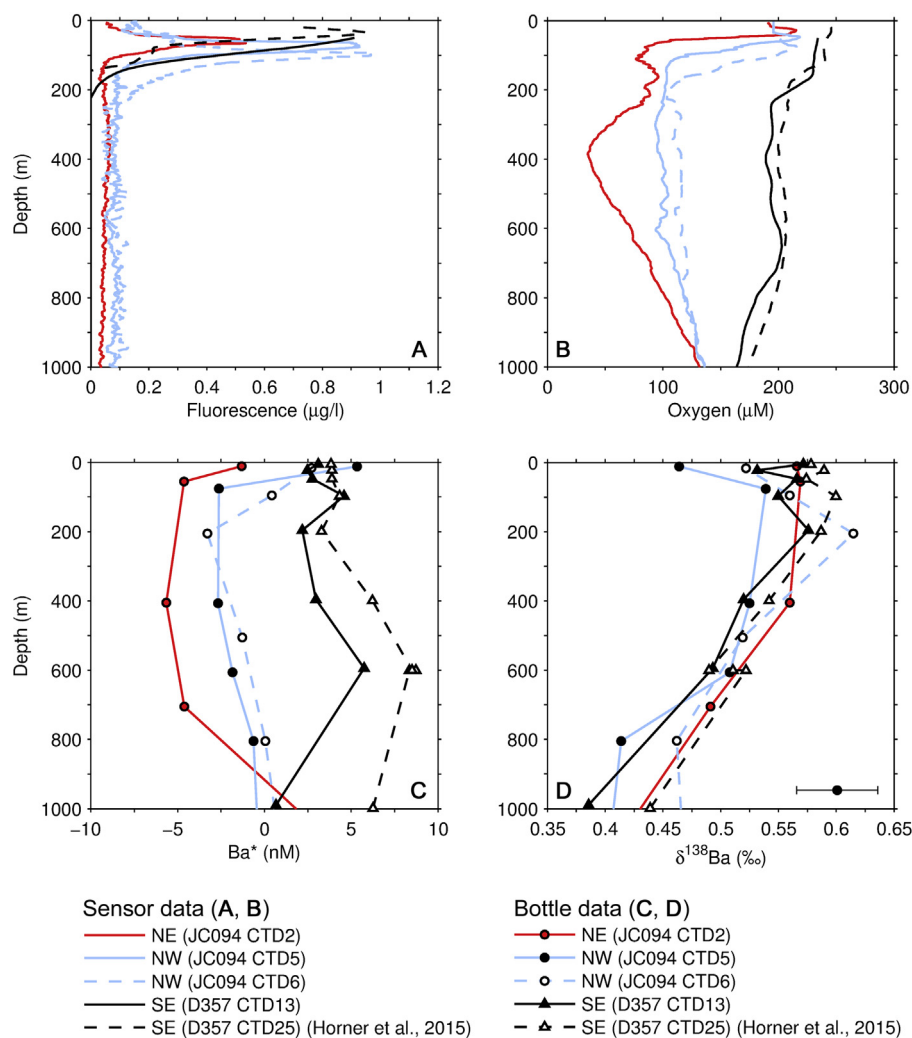
Fig. 5. Plots of (A) fluorescence, (B) oxygen, (C) Ba$^*$ and (D) $\delta^{138}$Ba in the top 1000 m at the different study sites. Tropical Atlantic data are plotted in red (eastern tropical) and blue (western tropical) with circle symbols, South Atlantic data are plotted in black with triangle symbols. Open triangle symbols and black dashed curves show previously-published data from the southeast Atlantic at 40°S (Horner et al., 2015) (see Fig. 2 for legend). Error bar shows representative ±2SD (±0.035 ‰). (For interpretation of the references to colour in this figure legend, the reader is referred to the web version of this article.)

ting the depth profile of Ba and Ba isotopes in the dissolved phase (Horner et al., 2015). Thus, neither the amount of nor depth of organic matter degradation (and so barite formation) can account for the trend towards lighter Ba isotope signatures towards the surface in the tropics, a feature that is absent from the South Atlantic profiles.

We suggest that the differences in the North and South Atlantic sub-surface water column profiles of Ba$^*$ and $\delta^{138}$Ba are as a result of the interplay between the physical structure of the upper water column and the vertical segregation of BaSO$_4$ and opal precipitation. Mixed layer depths (MLD) are shallower (less than 50 m) in the tropical Atlantic compared to the South Atlantic (maximum MLD greater than 100–150 m; Fig. 1), owing to a cap of low-density water in the Subtropics. Although both sampling events reported here were carried out in Oct–Nov, published MLD climatologies indicate that these MLDs

are likely to persist for the majority of the year (Kara et al., 2003). Regardless, if the MLD were to penetrate to the depths of barite formation, typically below 150 m (e.g. Dehairs et al., 2008; Jacquet et al., 2008), or able to entrain deeper waters that have experienced higher degrees of Ba removal into barite, the upper water column would be uniform for [Ba], Ba$^*$ and $\delta^{138}$Ba. The relatively constant [Ba], Ba$^*$ and $\delta^{138}$Ba observed in the uppermost ~200 m of the South Atlantic water column is thus consistent with periodic homogenisation of the upper water column by vertical mixing (Figs. 1 and 5).

In contrast, mixed layers in the tropical North Atlantic do not extend much below 50 m over an annual cycle (Fig. 1; Schmidtko et al., 2013). This range does not penetrate to the depths necessary to entrain Ba-depleted STUW (Subtropical Underwater; >200 m) or to those estimated for barite formation (>150 m). The STUW data are notable as

they exhibit significant decoupling of Ba and Si, first noted by Chan et al. (1977). This decoupling is clearly evident in the more negative values of $Ba^*$ in STUW compared to surface waters, implying Ba depletion relative to Si (Fig. 5C). More negative $Ba^*$ in STUW are also associated with $\sim+0.1\text{‰}$ increases in dissolved Ba isotope compositions relative to surface waters, consistent with the removal of isotopically-light Ba into $BaSO_4$ (e.g. Von Allmen et al., 2010). Such a pattern of more negative $Ba^*$ associated with heavier Ba isotope compositions in shallow subsurface waters is only expected if two conditions are met: if both the removal of Si and Ba are vertically segregated (e.g. via opal for Si and via $BaSO_4$ for Ba) and if the segregation remains protected from homogenisation via vertical mixing. As both of these conditions are satisfied in the STUW of the tropical North Atlantic, we conclude that the interplay between physical mixing and the vertical segregation of $BaSO_4$ and opal formation must be responsible for the differences between the profiles of $Ba^*$ and $\delta^{138}Ba$ in the tropical North and South Atlantic (Fig. 5).

### 4.3. Barium concentrations and isotopic variations in deep and intermediate waters

As with other elements that display nutrient-like behaviour, an important issue in understanding oceanic Ba cycling surrounds the relative contributions of conservative versus non-conservative Ba – the extent to which Ba distribution reflects simple mixing of different water masses versus *in situ* precipitation and dissolution. Since Ba is not directly cycled in association with organic matter (Sternberg et al., 2005), it is not possible to 'back-calculate' conservative Ba for a given water mass from other hydrographic parameters (e.g. using $O_2$ and *in situ* P; Broecker et al., 1985), thus requiring an alternative approach. A further complication arises when considering where the particles that are involved in dissolution processes originate from: some particles may arrive at depth from vertical sinking and some others from lateral transport. At depths below the MLD, our new profiles reveal key meridional and zonal differences that reflect the relative role of ocean circulation and barite dissolution in Ba cycling, both in deep waters ($\geq 2000$ m) and at intermediate depths (500–2000 m).

We investigated mixing processes by plotting our data in a mixing diagram, in which conservative mixing relationships will result in straight lines. The linear relationships shown in Fig. 6a illustrate that the tropical Atlantic Ocean $\delta^{138}Ba$-1/Ba systematics are consistent with conservative mixing being a major control below approximately 500 m, but also that statistically-significant differences exist between the tropical North and South Atlantic datasets (least squares fits to the data possess statistically-different intercepts and slopes for North and South Atlantic data). The different slopes of the mixing lines from the North

and South Atlantic may reflect a subtle overprint from *in situ* remineralisation of $BaSO_4$ and other Ba-bearing particles. This additional input of Ba would result in Ba-depleted (and initially isotopically heavy) deep waters from the North Atlantic exhibiting roughly similar Ba isotope compositions to Ba-replete water masses from equivalent depths in the South Atlantic, despite possessing significantly less Ba. Regardless, this effect is relatively small as the overall North Atlantic trend is linear (Fig. 6a), indicating that conservative mixing is the dominant control on Ba systematics in both the deep North and South Atlantic. Our Ba isotope data underscore the importance of conservative mixing as a control on Atlantic Ba cycling without the need to ratio to other biogeochemical tracers (e.g. [Si], $\underline{T}$, $S$). As we show in the next section however, we can use these additional tracers to independently constrain relative deep water mass mixing proportions, thus enabling us to estimate the Ba isotope compositions of the end-member northern- and southern-sourced water masses that mix in the deep Atlantic.

#### 4.3.1. Meridional overturning control of deep (>2000 m) Ba isotope distributions

The linear relationships between Ba isotope compositions and 1/Ba illustrate that conservative mixing accounts for essentially all of the Ba isotope variation in the deep Atlantic. Below 2000 m, the Atlantic is dominated by the mixing of nutrient-poor (and $O_2$-rich) northern-sourced waters (collectively termed NADW) with nutrient-rich southern-sourced bottom waters from the Weddell Sea (termed here AABW). Our data can be used to place constraints on the likely Ba isotope compositions of these two end-member water masses by independently calculating their relative mixing proportions. Broecker et al., 1991 suggested that the fraction of northern-sourced waters in a given sample, $f_n$, can be calculated using:

$$f_n = (1.67 - PO_4^*)/(1.67 - 0.73) \qquad (4)$$

where $PO_4^* = [PO_4^{3-}] + ([O_2]/175) - 1.95$. If we compare our Ba isotope data for samples below 2000 m against $f_n$ (Fig. 6b), we observe a distinct curvature that is indicative of a two-component hyperbolic isotopic mixing trend (e.g. Mariotti et al., 1988). In order to quantify the end-members responsible for generating the hyperbolic mixing trend, we make the simplifying assumption that there is no influence from non-conservative biogeochemical processes below 2000 m. Though this is likely an oversimplification, the strong linear (mixing) relationships shown in Fig. 6a indicate that mixing is certainly the dominant control on Ba isotope systematics in the deep Atlantic, despite barite being below saturation at these depths. As such, we can approximate the Ba isotope composition of a deep water mass purely in terms of mixing between northern- and southern-sourced waters:

$$\delta^{138/134}Ba_{insitu} = \frac{(f_n \times \delta^{138/134}Ba_n \times [Ba]_n) + ([1 - f_n] \times \delta^{138/134}Ba_s \times [Ba]_s)}{(f_n \times [Ba]_n) + ([1 - f_n] \times [Ba]_s)} \qquad (5)$$
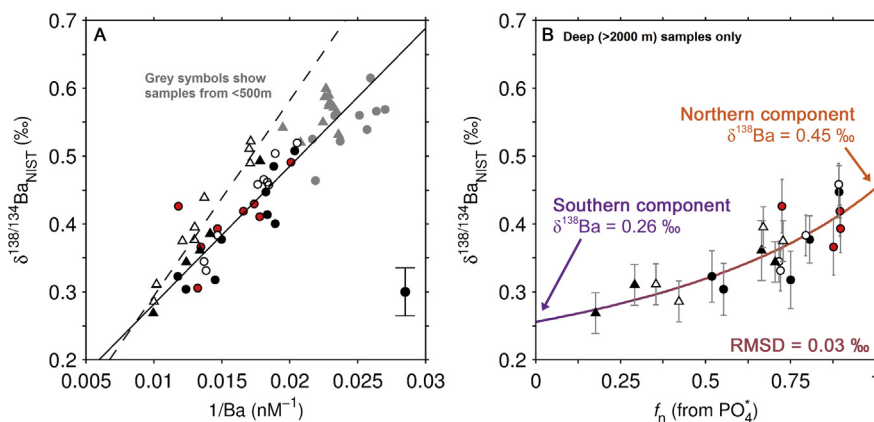
Fig. 6. (A) Mixing lines of $\delta^{138}Ba$ plotted against 1/Ba for the seawater samples from the tropical North Atlantic (circles) and the South Atlantic at approximately 40°S (triangles; Horner et al., 2015). Error bar shows representative ±2SD (±0.035‰). Least-squares linear regression lines are plotted separately for the tropical North Atlantic (solid line; $r^2 = 0.73$, $p < 0.05$) and South Atlantic (dashed line; $r^2 = 0.93$, $p < 0.05$) using data from ≥500 m. Grey symbols show samples from shallower than 500 m, which were not included in the regression calculation. (B) Calculated best-fit mixing line between northern- and southern-sourced water masses in the Atlantic below 2000 m (see text for calculation details). The excellent agreement between the simple mixing relationship and our seawater data suggest that it is possible to independently estimate $f_n$ from Ba isotope analyses using the relationship: $f_n \approx \frac{[21(50\delta^{138/134}Ba_{NIST}-13)]}{(550\delta^{138/134}Ba_{NIST}-48)}$ which is valid over the range of $\delta^{138/134}Ba_{NIST} = +0.26$ to $+0.45‰$; predictive error = 13%.

where $_n$ or $_s$ denote the northern- and southern-sourced end-members, respectively. The Ba concentration of the northern end-member was estimated to be 50 nM based on data from the Atlantic GEOSECS Expedition (average of Labrador Sea Water, Iceland-Scotland Overflow Water and Denmark Strait Overflow Water; Chan et al., 1977); the southern-sourced end-member was assigned [Ba] = 105 nM (based on Weddell Sea water; Hoppema et al., 2010).

Using the independent estimates of water mass mixing proportions from Eq. (3) and literature values of [Ba] for the northern- and southern-sourced end-members, we solved Eq. (4) for the Ba isotope compositions of the two end-members by minimisation of the data-line misfit, expressed as the RMSD (root-mean-square deviation; Fig. 6b). This calculation was restricted to the 21 samples from ≥2000 m and omitted sample #W0117 (JC094), as it possessed $f_n > 1$. The best-fit Ba isotope compositions for the northern- and southern-sourced water mass end-members were calculated as $\delta^{138/134}Ba_{NIST} = +0.45‰$ and +0.26‰, respectively. These two end-member compositions achieve a data-line RMSD of 0.03‰, roughly equivalent to our measurement precision of 0.03‰ for Ba-rich deep waters.

Importantly, this analysis suggests that the northern- and southern-sourced water masses that fill the deep Atlantic possess clearly-resolvable Ba isotope compositions ($\Delta^{138/134}Ba_{north-south} \approx 0.2‰$; Fig. 6b). If this pattern is verified throughout the Atlantic basin, Ba isotope analyses of deep waters may have utility in constraining '$f_n$' independently of existing methods. Moreover, if sedimentary archives that faithfully record deep water Ba isotope signals can be identified, Ba isotope analyses may enable temporal reconstruction of northern- versus southern-sourced waters in the deep ocean – and thus the geometry of overturning circulation – from a single biogeochemical tracer.

### 4.3.2. Zonal differences: influence from Labrador Sea Water at intermediate depths (500–2000 m)

A zonal (east–west) difference in Atlantic Ba concentrations and $\delta^{138}Ba$ systematics is suggested by differences between our tropical North Atlantic seawater profiles, centred at approximately 1500 m water depth (e.g. Fig. 3). In the western tropics (CTD005 and CTD006), Ba isotope compositions are ≈ +0.1‰ heavier than the values of $\delta^{138}Ba \approx +0.4‰$ seen in the eastern basin (CTD002; Fig. 3). These depths correspond to the depths of recently ventilated Upper Labrador Sea Water (ULSW) as shown by hydrographic data (nutrients, dissolved oxygen, and ventilation tracers such as radiocarbon; Chen et al., 2015; Jenkins et al., 2015). One possible interpretation for the elevated $\delta^{138/134}Ba$ in ULSW may relate to non-conservative processes, such as extensive barite formation or input of isotopically-heavy Ba in the Labrador Sea. Input of isotopically-heavy Ba into the Labrador Sea is unlikely since [Ba] is lower in ULSW compared to the equivalent water depths in the eastern tropical Atlantic (Fig. 3a). Similarly, the E–W difference in [Ba] is only ≈ 3 nM, and depth profiles of $Ba^*$ from the eastern and western North Atlantic show similar gradients, suggesting that extensive barite formation is unlikely to be responsible for removing significant quantities of Ba from the Labrador Sea. Moreover, non-conservative processes are largely precluded by the linear mixing relationships (Fig. 6a), suggesting that the isotopically-heavy Ba at the depths corresponding to ULSW are a conservative mixing feature. Thus, a simple explanation for this Ba isotope feature is that the influence from the advective inflow of ULSW is far greater in the western basin (CTD005, 006) compared to the eastern basin (CTD002), and that – since ULSW is recently-ventilated – this imparts an isotopically-heavy Ba signal at the depths where the influence from ULSW is greatest.

These subtle features in the depth profiles that are largely undetectable from examination of [Ba] illustrate that Ba isotope distributions are highly sensitive to ocean circulation, highlighting the possible utility of Ba isotopes as a powerful tracer of basin-scale hydrography in palaeoceanographic studies.

### 4.3.3. The sediment-water interface: a sedimentary source for dissolved Ba?

The limited number of near-bottom water samples collected from the tropical North Atlantic, in particular from the eastern basin, each show a slight deviation towards heavier $\delta^{138}$Ba at the very base of the profile (Fig. 3). We have no reason to believe that these signals are an analytical artefact or a blank issue for two reasons. Firstly, these samples were not atypical in other respects (e.g. $T$, $S$, $O_2$), suggesting that the bottles fired at the correct depths. Secondly, the Ba isotopic composition of the procedural Ba blank was measured as ~0‰ (Horner et al., 2015), whereas these bottom water samples exhibit shifts toward isotopically-heavy Ba of ~+0.4‰ rather than towards the isotopic composition of the blank. Our results hint towards a sedimentary source of dissolved Ba into these bottom waters since dissolved Ba *and* Ba$^*$ show significant upticks at the very base of the profiles, whereas a water mass signal would presumably also affect dissolved Si or other hydrographic parameters. The direction of the $\delta^{138}$Ba anomaly is opposite to that expected if the signature was a result of sinking barite, which would be expected to add Ba with an isotopic composition of ~+0.3‰ (assuming that BaSO$_4$ precipitates are approximately $-0.2$ to $-0.4$‰ lighter than mesopelagic waters; e.g. Von Allmen et al., 2010; Horner et al., 2015; Cao et al., 2016). Instead, this Ba may be sourced from seafloor sediments, which would indicate possible Ba isotopic fractionation effects during sediment diagenesis. Significant diffusive efflux of Ba from sediments under sulphate-reducing conditions has been previously noted (McManus et al., 1994; Hoppema et al., 2010), and could provide a possible mechanism for the apparent injection of isotopically-heavy Ba into overlying seawaters with lighter compositions. However, recent laboratory experiments (van Zuilen et al., 2016) have shown that diffusive transport results in a preferential release of isotopically-light Ba, and that adsorption preferentially retains isotopically-heavy Ba – both of these effects have the opposite fractionation factor to the patterns observed here. Clearly, further work into the nature of this isotopic enrichment is justified, including further field-based studies, given that sediments are a potentially important source of dissolved Ba to abyssal depths.

## 4.4. Synthesis: decoupling of barium concentration and isotopic composition in the Atlantic

### 4.4.1. A conceptual model for Ba cycling in the Atlantic

One of the key observations in our new data is that there is a stronger meridional variation in Ba concentrations compared to $\delta^{138}$Ba (Fig. 3). This apparent decoupling may be due to low fractionation of Ba during barite formation, resulting in relatively subtle variations in $\delta^{138}$Ba and a larger dissolved pool relative to particulate phases (Dehairs et al., 1991). Despite the overprint of barite remineralisation, Ba and $\delta^{138}$Ba variations can be traced along the meridional ocean circulation resulting in a conceptual model (Fig. 7) of the Ba cycle that is consistent with our new observations.

A greater concentration of Ba in southern-sourced mode waters in the tropics compared to 40°S is consistent with a gradual stripping of Ba in the upper mesopelagic layer (200–400 m) as a result of barite formation as the water mass is transported north by meridional circulation. Barite formation results in a small fractionation of Ba isotopes, resulting in the insignificant difference in $\delta^{138}$Ba between mode waters in the near-surface waters of the tropics compared to the South Atlantic, despite having undergone extensive Ba removal into BaSO$_4$ formation. In addition, there is also a re-entrainment of deeper water in the Equatorial upwelling regions, potentially allowing a certain degree of resetting on Ba isotope values. The rapid transit of water via LSW will also mean that samples in the mid-depths of the western basin will have heavier Ba isotopes and lower Ba concentrations than waters from the corresponding isopycnal in the eastern basin centred at approximately 1500 m. Similarly, NADW at 40°S has a greater Ba concentration than in the North Atlantic as a result of 'ageing' (barite dissolution, with a small contribution from the remineralisation of other Ba-bearing minerals e.g. celestite) along the meridional ocean circulation path and more AABW entrainment at depth.

### 4.4.2. Implications for the use of Ba-based proxies in palaeoceanography

Our Ba and $\delta^{138}$Ba depth profiles provide useful insights into the utility of carbonate Ba/Ca data as geochemical archives of ocean conditions. Firstly, the $\delta^{138}$Ba data from the North Atlantic are consistent with the formation of barite in subsurface waters, below 150 m, at the top of the mesopelagic layer rather than deeper in the water column, supporting the paradigm that barite formation occurs at similar depths associated with organic carbon remineralisation and export. Secondly, our data support the recently-advanced hypothesis that variations in the relationship between Ba, $\delta^{138}$Ba and dissolved Si are largely driven by ocean circulation and are set by the degree of barite formation in the subsurface waters of the high latitudes – where intermediate and deep waters are ventilated and subducted into the ocean interior (Horner et al., 2015). Small variations in the relationship between Ba and Si – quantified here using Ba$^*$ – point to Ba-specific overprinting through barite cycling, which imparts minor changes to Ba distributions but does not affect Si. However, these changes in Ba cycling are small relative to the overall structure of dissolved Ba and Si profiles, which are set by large-scale circulation processes. These observations suggest that geochemical archives of Ba, such as foraminiferal Ba/Ca, coupled together with proxies for marine silicon cycling, could shed light on changes in high-latitude carbon export and recycling. Moreover, reconstructions of deep ocean Ba isotopes could provide insight into the advective origin of water masses in the deep ocean and thus the geometry of the
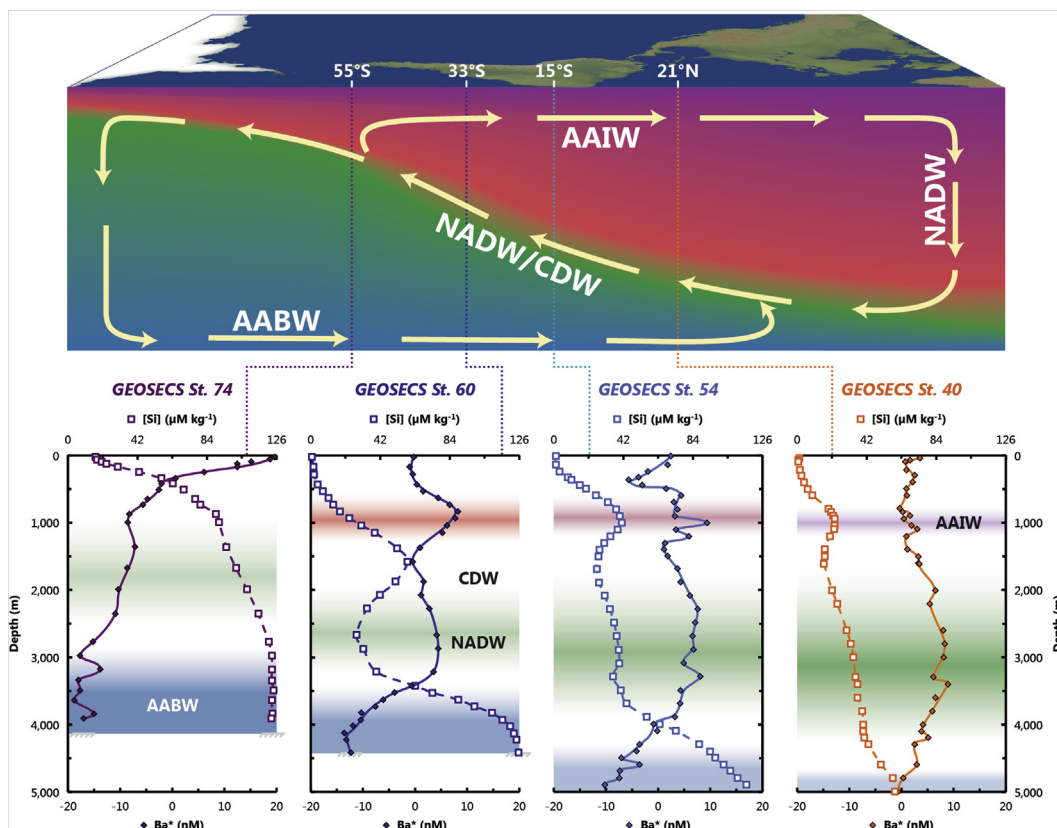
Fig. 7. Conceptual model of Ba cycling in the Atlantic. Southern component waters are enriched in Ba relative to Si. Southern-sourced intermediate/mode waters (i.e. AAIW) are gradually stripped of Ba as a result of barite formation and mixing as the water mass moves north, reducing Ba$^*$ but having minimal impact on $\delta^{138}$Ba. NADW/CDW at 40°S has a greater Ba concentration than in the North Atlantic as a result of barite dissolution and AABW entrainment during water mass ageing. (Fig. design by Jack Cook, Woods Hole Oceanographic Institution.)

meridional overturning circulation through time, subject to the identification of appropriate sedimentary archives.

## 5. CONCLUSION

We present four new full barium isotope depth profiles from the North and South Atlantic Ocean, allowing a robust assessment of both zonal and meridional Ba cycling across the Atlantic. Our data show that sub-surface barite formation results in heavy seawater $\delta^{138}$Ba at approximately 200–400 m depth, at the top of the mesopelagic layer, and that mesopelagic Ba isotope heterogeneity is likely determined by the depth of the mixed layer relative to that of barite formation. Below the depths of barite formation, Ba and $\delta^{138}$Ba systematics are mostly controlled by large-scale ocean circulation (i.e. conservative Ba cycling), with a subtle overprint from regenerated Ba that we attribute to *in situ* barite dissolution. We synthesise these findings to present a conceptual model of barium systematics in the Atlantic, which indicates that deep water barium concentrations and isotopic variations can be explained by conservative mixing between NADW and AABW with $\delta^{138}$Ba of the two end-members determined as +0.45 and +0.26 ‰, respectively. This mixing model suggests that Ba isotopes may facilitate tracing the proportion of northern- versus

southern-sourced waters filling the deep Atlantic in the geological past – and therefore the geometry of deep ocean circulation – from a single biogeochemical tracer. These results underscore the importance of large-scale mixing as the proximal cause of the strong correlation between dissolved Ba and Si in the Atlantic, thereby highlighting the utility of barium isotopes for understanding the processes governing marine Ba cycling. The use of Ba isotopes in marine chemistry thus harbours great promise as a new means to probe the mechanisms governing Ba-based tracers in palaeoceanography and how these relate to the temporal evolution of the oceans' biological carbon pump.

## APPENDIX A. SUPPLEMENTARY DATA

Supplementary data associated with this article can be found, in the online version, at http://dx.doi.org/10.1016/j.gca.2017.01.043.

## REFERENCES

Bertram M. A. and Cowen J. P. (1997) Morphological and compositional evidence for biotic precipitation of marine barite. *J. Mar. Res.* **55**, 577–593.

Bishop J. (1989) Regional extremes in particulate matter composition and flux: effects on the chemistry of the ocean interior. *Productivity of the ocean: present and past* **44**, 117–137.

Böttcher M. E., Geprägs P., Neubert N., Von Allmen K., Pretet C., Samankassou E. and Nägler T. F. (2012) Barium isotope fractionation during experimental formation of the double carbonate BaMn [CO$_3$]$_2$ at ambient temperature. *Isot. Environ. Health Stud.* **48**, 457–463.

Brewer P. and Riley J. (1965) The Automatic Determination of Nitrate in Sea Water, Deep Sea Research and Oceanographic Abstracts. *Elsevier*, 765–772.

Broecker W. S., Blanton S., Smethie W. M. and Ostlund G. (1991) Radiocarbon decay and oxygen utilization in the deep Atlantic Ocean. *Global Biogeochem. Cycles* **5**, 87–117.

Broecker W. S. and Peng T.-H. (1982) *Tracers in the Sea*. Eldigio Press.

Broecker W. S., Takahashi T. and Takahashi T. (1985) Sources and flow patterns of deep-ocean waters as deduced from potential temperature, salinity, and initial phosphate concentration. *J. Geophys. Res. C: Oceans* **90**, 6925–6939.

Brzezinski M. A., Sigman D. M., Sarmiento J. L., Matsumoto K., Gruber N., Rau G. H. and Coale K. H. (2002) A switch from Si (OH)$_4$ to NO$_3^-$ depletion in the glacial Southern Ocean. *Geophys. Res. Lett.* **29**, 1564.

Cao Z., Siebert C., Hathorne E. C., Dai M. and Frank M. (2016) Constraining the oceanic barium cycle with stable barium isotopes. *Earth Planet. Sci. Lett.* **434**, 1–9.

Cardinal D., Savoye N., Trull T. W., André L., Kopczynska E. E. and Dehairs F. (2005) Variations of carbon remineralisation in the Southern Ocean illustrated by the Ba xs proxy. *Deep Sea Res. Part I* **52**, 355–370.

Carritt D. E. and Carpente J. (1966) Comparison and evaluation of currently employed modifications of Winkler method for determining dissolved oxygen in seawater-a NASCO Report. *J. Mar. Res.* **24**, 286-&.

Chan L. H., Drummond D., Edmond J. M. and Grant B. (1977) On the barium data from the Atlantic GEOSECS expedition. *Deep Sea Res.* **24**(7), 613–649.

Chen T., Robinson L. F., Burke A., Southon J., Spooner P., Morris P. J. and Ng H. C. (2015) Synchronous centennial abrupt events in the ocean and atmosphere during the last deglaciation. *Science* **349**, 1537–1541.

Collier R. and Edmond J. (1984) The trace element geochemistry of marine biogenic particulate matter. *Prog. Oceanogr.* **13**, 113–199.

Craig H. and Turekian K. (1980) The GEOSECS program: 1976–1979. *Earth Planet. Sci. Lett.* **49**, 263–265.

Cutter G., Andersson P., Codispoti L., Croot P., Francois R., Lohan M., Obata H. and Rutgers vd Loeff M. (2010) Sampling and sample-handling protocols for GEOTRACES Cruises.

Dehairs F., Chesselet R. and Jedwab J. (1980) Discrete suspended particles of barite and the barium cycle in the open ocean. *Earth Planet. Sci. Lett.* **49**, 528–550.

Dehairs F., Jacquet S., Savoye N., Van Mooy B. A., Buesseler K. O., Bishop J. K., Lamborg C. H., Elskens M., Baeyens W. and Boyd P. W. (2008) Barium in twilight zone suspended matter as a potential proxy for particulate organic carbon remineralization: Results for the North Pacific. *Deep Sea Res. Part II* **55**, 1673–1683.

Dehairs F., Stroobants N. and Goeyens L. (1991) Suspended barite as a tracer of biological activity in the Southern Ocean. *Mar. Chem.* **35**, 399–410.

Dymond J., Suess E. and Lyle M. (1992) Barium in deep-sea sediment: A geochemical indicator of paleoproductivity. *Paleoceanography* **7**, 163–181.

Eagle M., Paytan A., Arrigo K. R., van Dijken G. L. and Murray R. W. (2003) A comparison between excess barium and barite as indicators of carbon export. *Paleoceanography* **18**. Art no.: 1021.

Foster D. A., Staubwasser M. and Henderson G. M. (2004) 226 Ra and Ba concentrations in the Ross Sea measured with multi-collector ICP mass spectrometry. *Mar. Chem.* **87**, 59–71.

Ganeshram R. S., Francois R., Commeau J. and Brown-Leger S. L. (2003) An experimental investigation of barite formation in seawater. *Geochim. Cosmochim. Acta* **67**, 2599–2605.

Gingele F. and Dahmke A. (1994) Discrete barite particles and barium as tracers of paleoproductivity in South Atlantic sediments. *Paleoceanography* **9**, 151–168.

González-Munoz M. T., Fernández-Luque B., Martínez-Ruiz F., Chekroun K. B., Arias J. M., Rodríguez-Gallego M., Martínez-Canamero M., De Linares C. and Paytan A. (2003) Precipitation of barite by Myxococcus xanthus: possible implications for the biogeochemical cycle of barium. *Appl. Environ. Microbiol.* **69**, 5722–5725.

Grasshoff K., Kremling K. and Ehrhardt M. (1999) *Methods of Seawater Analysis*. John Wiley & Sons.

Griffith E. M. and Paytan A. (2012) Barite in the ocean–occurrence, geochemistry and palaeoceanographic applications. *Sedimentology* **59**, 1817–1835.

Gruber N. and Sarmiento J. L. (1997) Global patterns of marine nitrogen fixation and denitrification. *Global Biogeochem. Cycles* **11**, 235–366.

Hall J. M. and Chan L.-H. (2004a) Ba/Ca in benthic foraminifera: thermocline and middepth circulation in the North Atlantic during the last glaciation. *Paleoceanography* **19**. Art no.: PA4018.

Hall J. M. and Chan L.-H. (2004b) Ba/Ca in Neogloboquadrina pachyderma as an indicator of deglacial meltwater discharge into the western Arctic Ocean. *Paleoceanography* **19**. http://dx.doi.org/10.1029/2003PA000910.

Hernandez-Sanchez M. T., Mills R. A., Planquette H., Pancost R. D., Hepburn L., Salter I. and FitzGeorge-Balfour T. (2011) Quantifying export production in the Southern Ocean: Implications for the Baxs proxy. *Paleoceanography* **26**.

Hoefs J. (2015) Isotope Fractionation Processes of Selected Elements, Stable Isotope Geochemistry. *Springer*, 47–190.

Hoppema M., Dehairs F., Navez J., Monnin C., Jeandel C., Fahrbach E. and De Baar H. (2010) Distribution of barium in the Weddell Gyre: Impact of circulation and biogeochemical processes. *Mar. Chem.* **122**, 118–129.

Horner T. J., Kinsley C. W. and Nielsen S. G. (2015) Barium-isotopic fractionation in seawater mediated by barite cycling and oceanic circulation. *Earth Planet. Sci. Lett.* **430**, 511–522.

Jacquet S., Dehairs F., Elskens M., Savoye N. and Cardinal D. (2007) Barium cycling along WOCE SR3 line in the Southern Ocean. *Mar. Chem.* **106**, 33–45.

Jacquet S., Dehairs F., Savoye N., Obernosterer I., Christaki U., Monnin C. and Cardinal D. (2008) Mesopelagic organic carbon remineralization in the Kerguelen Plateau region tracked by biogenic particulate Ba. *Deep Sea Res. Part II* **55**, 868–879.

Jenkins W., Smethie W., Boyle E. and Cutter G. (2015) Water mass analysis for the US GEOTRACES (GA03) North Atlantic sections. *Deep Sea Res. Part II* **116**, 6–20.

Kara A. B., Rochford P. A. and Hurlburt H. E. (2003) Mixed layer depth variability over the global ocean. *J. Geophys. Res. C: Oceans* **108**.

Kirkwood D. (1989) Simultaneous determination of selected nutrients in sea water. International Council for the Exploration of the Sea (ICES) CM 100, 29.

Lea D. W. and Boyle E. A. (1989) Barium content of benthic foraminifera controlled by bottom-water composition. *Nature* **338**, 751–753.

Lea D. W. and Boyle E. A. (1991) Barium in planktonic foraminifera. *Geochim. Cosmochim. Acta* **55**, 3321–3331.

Mariotti A., Landreau A. and Simon B. (1988) 15 N isotope biogeochemistry and natural denitrification process in groundwater: Application to the chalk aquifer of northern France. *Geochim. Cosmochim. Acta* **52**(7), 1869–1878.

McManus J., Berelson W. M., Klinkhammer G. P., Kilgore T. E. and Hammond D. E. (1994) Remobilization of barium in continental margin sediments. *Geochim. Cosmochim. Acta* **58**, 4899–4907.

Miyazaki T., Kimura J.-I. and Chang Q. (2014) Analysis of stable isotope ratios of Ba by double-spike standard-sample bracketing using multiple-collector inductively coupled plasma mass spectrometry. *J. Anal. At. Spectrom.* **29**, 483–490.

Monnin C., Jeandel C., Cattaldo T. and Dehairs F. (1999) The marine barite saturation state of the world's oceans. *Mar. Chem.* **65**, 253–261.

Nan X., Wu F., Zhang Z., Hou Z., Huang F. and Yu H. (2015) High-precision barium isotope measurements by MC-ICP-MS. *J. Anal. At. Spectrom.* **30**, 2307–2315.

Nelson D. M., Treguer P., Brzezinski M. A., Leynaert A. and Queguiner B. (1995) Production and dissolution of biogenic silica in the ocean: revised global estimates, comparison with regional data and relationship to biogenic sedimentation. *Global Biogeochem. Cycles* **9**, 359–372.

Nurnberg C. C., Bohrmann G., Schluter M. and Frank M. (1997) Barium accumulation in the Atlantic sector of the Southern Ocean: results from 19,000 year records. *Paleoceanography* **12**, 594–603.

Paytan A. and Kastner M. (1996) Benthic Ba fluxes in the central Equatorial Pacific, implications for the oceanic Ba cycle. *Earth Planet. Sci. Lett.* **142**, 439–450.

Riebesell U., Schulz K. G., Bellerby R., Botros M., Fritsche P., Meyerhöfer M., Neill C., Nondal G., Oschlies A. and Wohlers J. (2007) Enhanced biological carbon consumption in a high $CO_2$ ocean. *Nature* **450**, 545–548.

Robinson L. F. (2014) RRS James Cook Cruise JC094, October 13–November 30 2013, Tenerife-Trinidad. TROPICS, Tracing Oceanic Processes using Corals and Sediments. Reconstructing abrupt Changes in Chemistry and Circulation of the Equatorial Atlantic Ocean: Implications for global Climate and deep-water Habitats.

Sarmiento J. L., Gruber N., Brzezinski M. A. and Dunne J. P. (2004) High-latitude controls of thermocline nutrients and low latitude biological productivity. *Nature* **427**, 56–60.

Schlitzer R. (2000) Electronic atlas of WOCE hydrographic and tracer data now available. EOS Trans, AUG 81, 45.

Schmidtko S., Johnson G. C. and Lyman J. M. (2013) MIMOC: A global monthly isopycnal upper-ocean climatology with mixed layers. *J. Geophys. Res. C: Oceans* **118**, 1658–1672.

Siebert C., Nagler T. F. and Kramers J. D. (2001) Determination of molybdenum isotope fractionation by double-spike multicollector inductivity coupled plasma mass spectrometry. *Geochem. Geophysics Geosystems* **2**. http://dx.doi.org/10.1029/2000GC000124.

Sternberg E., Tang D., Ho T.-Y., Jeandel C. and Morel F. M. (2005) Barium uptake and adsorption in diatoms. *Geochim. Cosmochim. Acta* **69**, 2745–2752.

Talley L. D. (2013) Closure of the global overturning circulation through the Indian, Pacific, and Southern Oceans: Schematics and transports. *Oceanography* **26**, 80–97.

Talley L. D., Pickard G. L., Emery W. J. and Swift J. H. (2011) *Descriptive Physical Oceanography: An Introduction*. Academic Press.

Tilstone G. H., Taylor B. H., Blondeau-Patissier D., Powell T., Groom S. B., Rees A. P. and Lucas M. I. (2015) Comparison of new and primary production models using SeaWiFS data in contrasting hydrographic zones of the northern North Atlantic. *Remote Sens. Environ.* **156**, 473–489.

Tréguer P. and De la Rocha C. L. (2013) The world ocean silica cycle. *Annu. Rev. Mar. Sci.* **5**, 477–501.

van Zuilen K., Müller T., Nägler T. F., Dietzel M. and Küsters T. (2016) Experimental determination of barium isotope fractionation during diffusion and adsorption processes at low temperatures. *Geochim. Cosmochim. Acta* **186**, 226–241.

Varela D. E., Pride C. J. and Brzezinski M. A. (2004) Biological fractionation of silicon isotopes in Southern Ocean surface waters. *Global Biogeochem. Cycles* **18**. http://dx.doi.org/10.1029/2003GB002140.

Von Allmen K., Böttcher M. E., Samankassou E. and Nägler T. F. (2010) Barium isotope fractionation in the global barium cycle: First evidence from barium minerals and precipitation experiments. *Chem. Geol.* **277**, 70–77.

Zhang J.-Z. and Chi J. (2002) Automated analysis of nanomolar concentrations of phosphate in natural waters with liquid waveguide. *Environ. Sci. Technol.* **36**, 1048–1053.

*Associate editor:* Daniel Sinclair